ISSN 1392–1207. MECHANIKA. 2014 Volume 20(5): 447–451

Mechanical properties and cyclic fracture behavior of differently heat-treated steel

M. Leonavičius*, E. Stupak, G. Petraitis*****
**Vilnius Gediminas Technical University, Saulėtekio 11, 10223 Vilnius, Lithuania,*
E-mail: mindaugas.leonavicius@vgtu.lt
***Vilnius Gediminas Technical University, Saulėtekio 11, 10223 Vilnius, Lithuania, E-mail: eugenius.stupak@vgtu.lt*
****Vilnius Gediminas Technical University, Saulėtekio 11, 10223 Vilnius, Lithuania, E-mail: gediminas.petraitis@vgtu.lt*

crossref http://dx.doi.org/10.5755/j01.mech.20.5.7392

1. Introduction

For mining equipment structural elements such as gears and bolts the specific requirements are applied. Gears must be of sufficient strength with high surface hardness (preferred 280-320 HRB) in order to resist wear but remain ductile in deeper layers, have a good weldability and be easily processed and be fairly light. While for the threads the large localised concentration zones arise. Therefore in this case it is important that the threshold stress intensity factor range was as higher. When there is a need of providing the elements with those properties the heat treatment shall be applied. Medium carbon low alloyed steel grade AISI 4130 meet those requirements due to controllable heat-treatment processes and good mechanical processability and is widely used for this industry [1-7].

The research includes the determination of influence of hardening with high tempering and normalisation on steel's AISI 4130 static, dynamic and cyclic properties.

2. Material and heat treatment

For the experiment two kinds of steel grade 4130 was used, produced in different foundries. Chemical composition is presented in Table.

Table

Chemical composition (in weight %)

	Cr	Mo	C	Mn	P	S	Si
St-1	0.8-1.1	0.15-0.25	0.28-0.33	0.4-0.6	0.035	0.04	0.15-0.35
St-2	0.8-1.1	0.15-0.25	0.28-0.33	0.7-0.9	0.035	0.04	0.15-0.35

Note that chemical composition slightly differs. Manganese amount was 0.4 ... 0.6% in St-1 and 0.7 ... 0.9% in St-2 respectively. The larger amount of manganese determines finer ferrite grains and shape [3, 4], and improve the mechanical and cyclic strength properties.

Heat treatment of the both steels was different. St-1 – hardening with high tempering (austenitized at 870°C and quenched in oil, then tempered at 650°C to receive required hardness). Hardening with high tempering is applied in order to obtain the required hardness at element's working parts, but also enables to maintain a high strength necessary for gears. During hardening the steel is heated up to austenitizing structure then is cooled in oil. During tempering it is heated up to 650°C temperature, hold at it and slowly cooled in the air. Tempering temperature was chosen in order to obtain the desired hardness in the range of 280-320 HRC. Microstructure of the steel consisted of ferrite and pearlite (white and dark areas), and is shown in Fig. 1, a.

The heat treatment of St-2 was normalization (austenitizing at 870°C, temperature 30-50°C higher than austenitizing temperature and air cooling to room). It was attempt by normalization to obtain fine grained structure of steel whose hardness and strength should be slightly higher than after annealing. Normalized steel's structure consisted of fine grained pearlite and ferrite, and is shown in Fig. 1, b. Structure has a slight banding.

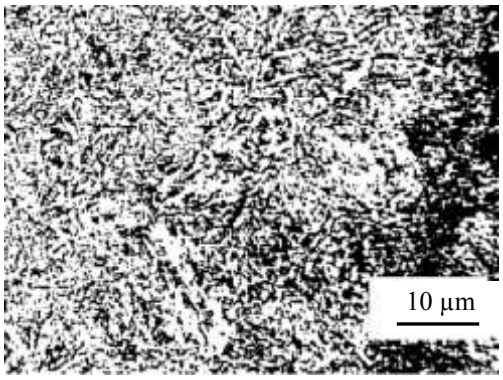

a

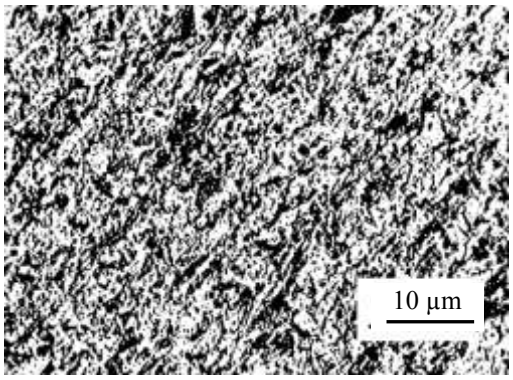

b

Fig. 1 Microstuctures of St-1 (a) and St-2 (b)

3. Mechanical and dynamic properties

St-1 static mechanical properties were determined by testing round tensile specimens (d = 8 mm), made of CT specimens after their cyclic tests. Determined mechanical properties are as in Table 2. St-1 hadn't the yield point, therefore the 0.2% offset yield strength was determined. Hardness BHN = 288 ... 299 – slightly ranges and satisfy the values required for gears.

Table 2

Mechanical properties

	R_{eL}, MPa	R_m, MPa	E, GPa	Z, %
St-1	776 ... 778	938 ... 942	181 ... 185	58.8 ... 59.9
St-2	400 ... 564	640 ... 732	189 ... 201	61.7 ... 62.3

Cutting scheme of round and CT specimens of St-2 is shown in Fig. 2, a. Hardness determined for each specimen varies insignificantly BHN = 197 ... 206. Larger hardnesses are of those specimens which were processed from near of the workpieces edge. Round specimens (Fig. 2, b) were processed of near the workpieces edge and of CT specimen from near the workpieces centre after its cyclic tests (d = 8 mm) shown in Fig. 2, b. Tensile diagrams of St-1 and St-2 are shown in Fig. 3.

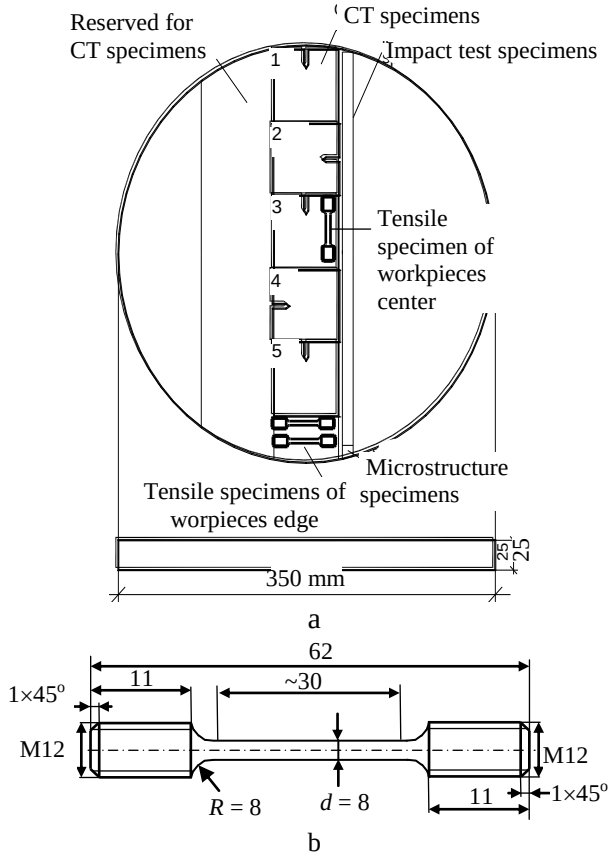

Fig. 2 Specimens preparation schemme of St-2 (a), and round specimen (b)

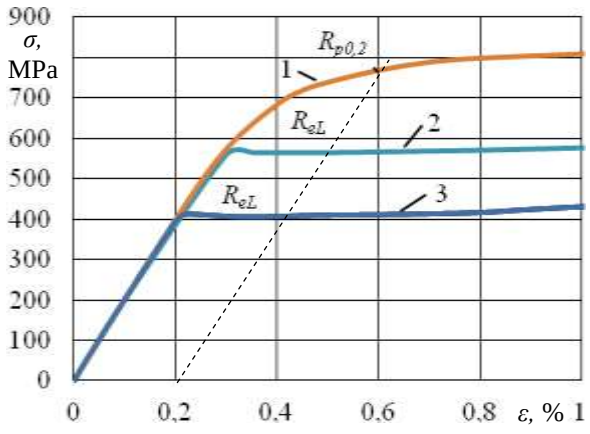

Fig. 3 Stress strain curves: *1* – St-1; *2* – St-2, workpiece edge; *3* – St-2, centre

Large dispersal of the values is explained by the fact that the workpiece for specimens was cut off from rolled steel beam, for which due to large dimensions it was difficult to ensure uniform heat transfer during heat treatment procedure. Larger determined values were of specimens of superficial layer, the smaller ones are of specimens cut off in around near the workpieces centre.

The Charpy notch type (10 x10) specimens for impact tests were made of workpieces. Determined impact tests indicators varies noticeably: St-1 KCV = 28.1 ... 32.0 J; St-2 – KCV = 44.9 ... 78.2 J. The indicators of St-2 are 1.4 ... 2.5 times larger than are of St-1. The fractures of impact test specimens are shown in Fig. 4.

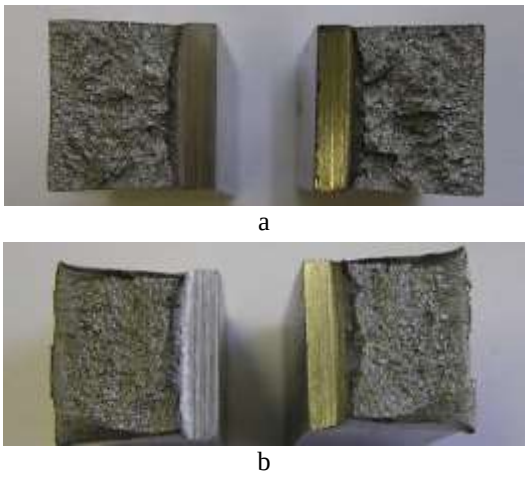

Fig. 4 Halves of broken Charpy notch type impact test specimens of St-1 (a) and St-2 (b)

4. Resistance to cyclic loading

Resistance to cyclic loading was determined according to ASTM E 647-93. In CT specimens, by applying cyclic loading, the crack is grown up, which is periodically stopped up to defined crack propagation rates. By the above referred methodises the crack is stopped until crack propagation rate decreases up to 10^{-10} m/cycle [8, 9]. In order to apply the obtained results for larger operational longevity in this work the threshold was fixed at crack propagation rate less than 10^{-11} m/cycle.

Compact tension specimens (CT) for determination of stress intensity factor K were produced from both steels. CT specimen is presented in Fig. 5. St-1 specimens were made of specially prepared plate, and the cutting scheme of St-2 CT specimens is presented in Fig. 2. The notch for each specimen was made in different direction.

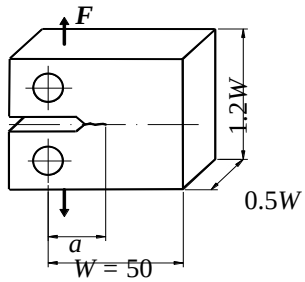

Fig. 5 CT specimen

The stress intensity factor $\Delta K = K_{max} - K_{min}$ was calculated by ASTM E 647-00 formula:

$$K = \left(F / W^{1/2}\right) f(\lambda) \quad (1)$$

$$\text{where } f(\lambda) = \frac{2+\lambda}{(1-\lambda)^{\frac{3}{2}}}\left[\begin{matrix}0.866 + 4.64\lambda - 13.32\lambda^2 + \\ +14.72\lambda^3 - 5.6\lambda^4\end{matrix}\right] \quad (2)$$

$\lambda = a/W$, F is tensile force, B is specimen's thickness, W is specimen's basis, a is crack size.

Dependencies of steel St-1 crack propagation rate da/dN versus stress intensity factor range ΔK are presented in reference [7]. Obtained threshold values are: ΔK_{th} = 7.3 ... 8.8 MPa·√m for $da/dN = 10^{-10}$ m/cycle and ΔK_{th} = 7.1 ... 8.6 MPa·√m for $da/dN < 10^{-11}$ m/cycle.

Same dependencies for five specimens made of steel St-2 are presented in Fig. 6. Obtained threshold values are: ΔK_{th} = 10.7 ... 11.8 MPa √m for da/dN = $= 10^{-10}$ m/cycle and ΔK_{th} = 9.3 ... 10.6 MPa √m for $da/dN < 10^{-11}$ m/cycle.

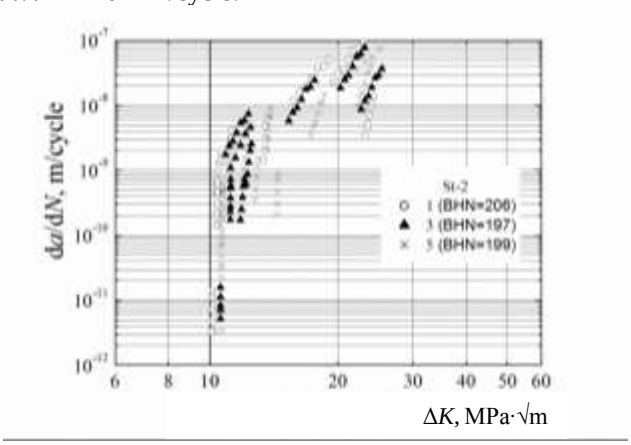

a

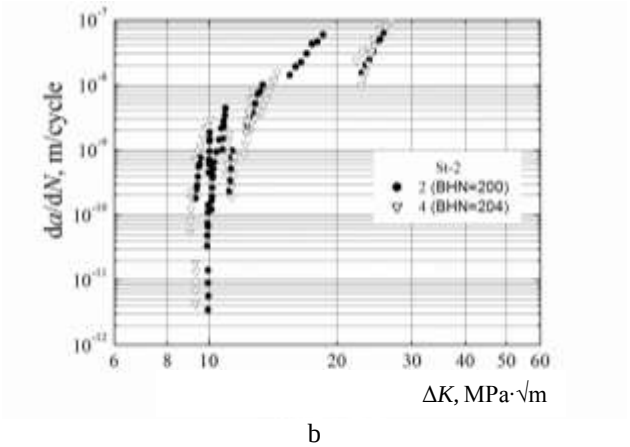

b

Fig. 6 Diagrams for St-2 specimens 1, 3, 5 (a) and 2, 4 (b)

According to the data [7] and Fig. 6 the dependencies of threshold stress intensity factor range on ultimate stress R_m and yield limit $R_{el}(R_{0.2})$ ratio (Fig. 7, a); and hardness (Fig. 7, b) are constructed for both steels. From the data it is clear that ΔK_{th} increases due to increased plasticity. Values of ΔK_{th} for steel St-2 increases for decreasing hardness in comparison with steel St-1.

After the threshold stress intensity factor determination tests the CT specimens were tested for the fracture toughness. If the stress-strain state at the vicinity of crack tip becomes critical, the sudden fracture arises. The critical stress-strain state is described by parameter K_{IC} (fracture toughness), which quantitatively evaluates the material's property to resist brittle fracture. Fracture toughness is obtained according to the standard ASTM E 399-83 [8].

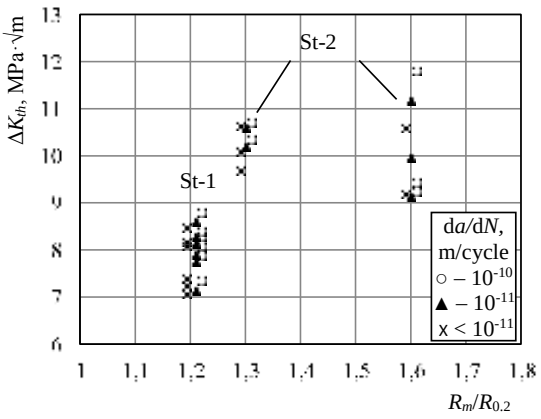

a

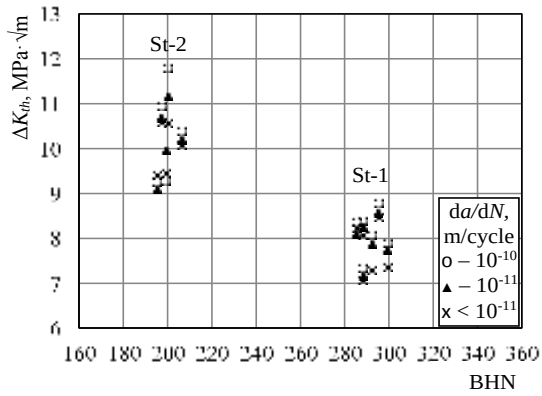

b

Fig. 7 Dependence of threshold stress intensity factor range on plasticity (a) and hardness (b)

The curves of fracture toughness determination test are presented in Fig. 8. Curve „1" is of St-1 specimens. This curve is II standard type crack opening diagram [9], with the force F_{max} between lines 0-a and 0-b and $F_{max} = F_Q$. Curve „2" is of St-2 specimen is a I type diagram, where the forcevalue is as $F_5 = F_Q$.

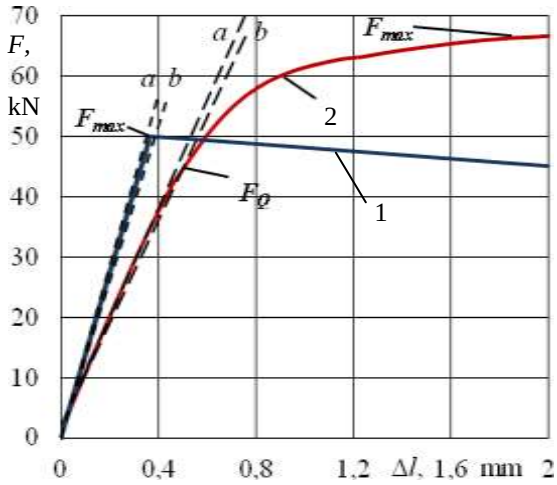

Fig. 8 Fracture toughness test curves: *1* – St-1; *2* – St-2

Value of critical stress intensity factor K_C is determined using formulas (1) and (2). It can be used as parameter of fracture toughness K_{IC} if four additional conditions are fulfilled; if conditions are not satisfied then instead of K_{IC} the K_C is determined. In all specimens of St-1 crack size is out of the range of $0.45W \le a \le 0.55W$, so the values of K_C were determined and had spread in the range from 51.3 up to 74.9 MPa·√m. For St-2 specimens requirement of $F_{max}/F_Q \le 1.1$ was not satisfied, and also the K_C were determined and ranged from 75.6 up to 86.2 MPa·√m.

In order to obtain better understanding of fatigue crack propagation fractured views were examined in optic microscopy (Fig. 9) and scanning electron microscopy (SEM) as presented in Fig. 10 and Fig. 11.

Fractured micrographs of CT specimens are presented in Fig. 9. Tonques initiated near to the few cracks origins are observed in the influence zone of the notch. Further the tonques coalescence into the main crack after its length reached approximately 3 mm. In fatigue zone the tunneling effect was observed caused by stress-strain state. Zone of static break for selected St-1 specimen is as brittle-to-ductile shape, for other specimens also. For St-2 this zone is mainly brittle, but in the part between fatigue zone and static zone ductile fracture signs and tunneling effects are observed. The flutes seen on the CT fractures (Fig. 9) are obtained due to the load decreasing procedure used for threshold determination.

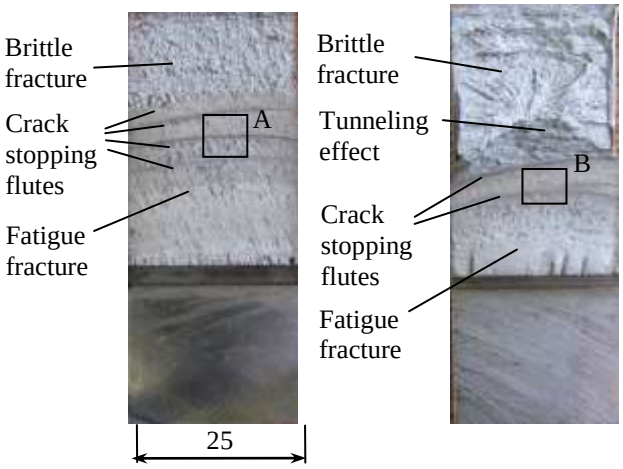

Fig. 9 Fractures of specimens: a) St-1; b) St-2

Magnified fractures of St-1 specimen are presented in Fig. 10. Round- and oval shaped dimples are observed in fatigue zone perpendicular to crack propagation front. It is a crystals of pearlite or its groups. In the view presented in Fig. 10, a one could observe inclusions of heterogeneities which consist of nitrides, oxides, carbides and sulphides. In these places dominate flakes – round shaped or elliptical internal voids, which are as silver colour flakes in the break as presented in Fig. 10, b. It makes influence for crack propagation and change size and direction of fatigue striations.

Views of St-2 specimen 4th (Fig. 9, b) fatigue zone are presented in Fig. 11, where brittle-to-ductile fracture mechanism is observed. Fatigue striations, broken crystals (caused due to granular and intergranular fracture), failure facets, differently sized and shaped dimples are observed. Larger and deeper material destructions, wider dimples are caused by non-metallic inclusions between grains of different size. Fractured views of tension specimens, CT and Charpy specimens (macro- and micro-mechanisms of failure of specimens cut of the CCM roll surface with crack-like defects [10, 11]) are compared with material microstructure, described by different sized and shaped crystals of ferrite and pearlite, various inhomogeneities effecting static, dynamic and cyclic fracture.

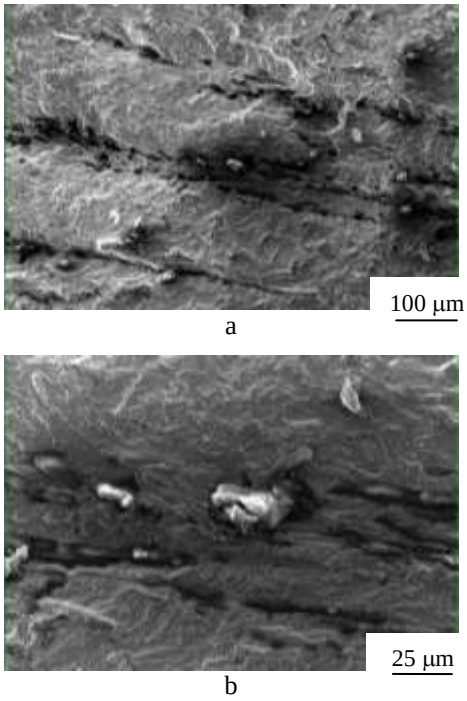

Fig. 10 SEM views of St-1 fracture: a – zoom near "A" (Fig. 9, a); b – flakes illustration

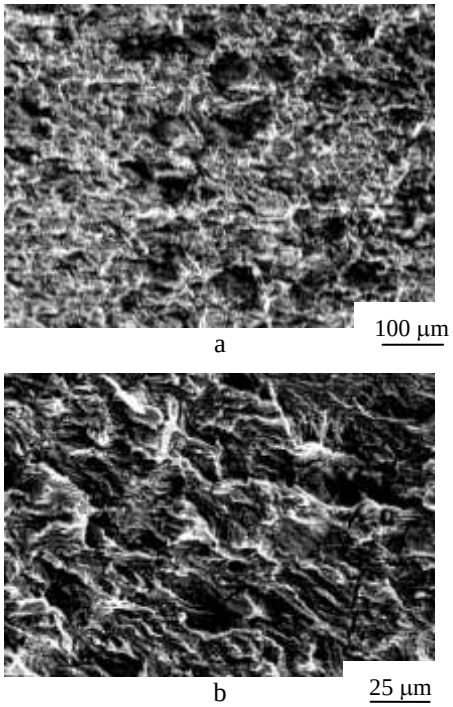

Fig. 11 SEM views of St-2 fracture: a – zoom near "B" (Fig. 9, b); b – enlarged

Insignificant change of chemical content, heat-treatment allowed to obtain materials usable for structural elements with different functionality.

5. Conclusions

1. Low carbon steel AISI 4130 used for evaluation of suitability for parts of mining equipment was prepared in order to determine an influence of thermal treatment on mechanical, dynamic properties; and cyclic resistance. The analysis revealed that above mentioned properties are spread in a wide range.

2. Static mechanical properties show that steel's St-2 tensile strength R_m = 640 ... 732 MPa is less in comparison with the steel's St-1 tensile strength R_m = 938 ... 942 MPa. The yield stress is also less but the plasticity is higher.

3. Determined values of resistance KCV to impact loading obtained by Charpy specimens: for steel St-1 are 28.1 … 32.0 J; and for St-2 are 44.9 ... 78.2 J, spread is caused by inhomogeneous microstructure of material.

4. Steel's St-2 threshold at low crack propagation rates $da/dN < 10^{-11}$ m/cycle is ΔK_{th} = 9.3 ... 10.6 MPa·√m and is approximately 20 % larger than it is of St-1 ΔK_{th} = 7.1 ... 8.8 MPa·√m.

Acknowledgments

The study was supported by CERC of VGTU.

References

1. **Rudnev, V.; Loveless, D.; Cook, R.; Black, M.** 2003. Induction hardening of gears: a review, Heat treatment of metals 9: 97-103.
2. **Davis, J.R.** 2005. Gear materials, properties, and manufacture. ASM International. 339p.
3. **Philip, T.V.** 1999. Ultrahigh-strength steels. ASM handbook, Volume 1, Properties and selection: Irons, steels, and high performance alloys, in ASM Handbook on CD-ROM, ASM International and The Dialog Corporation. Retrieved December 2, 2003.
4. **Rice, R.C., Jackson, J.L., Bakuckas, J.; Thompson, S.** 2003. Metallic materials properties development and standardization (MMPDS), U.S. Department of Transportation/Federal Aviation Administration Report, 2.10-2.38.
5. **Song, R.; Ponge, D.; Raabe, D.** 2005. Influence on Mn content on the microstructure and mechanical properties of ultrafine grained C-Mn steels, ISIJ International 45(11): 1721-1726. http://dx.doi.org/10.2355/isijinternational.45.1721.
6. **Rajan, K.M., Deshpande, P.U.; Narasimhan, K.** 2002. Effect of heat treatment of preform on the mechanical properties of flow formed AISI 4130 steel tubes – a theoretical and experimental assessment, J. of Materials Processing Technology 125-126: 503-511. http://dx.doi.org/10.1016/S0924-0136(02)00305-9.
7. **Bobyliov, K.; Leonavičius, M.; Šukšta, M.; Krenevičius, A.; Stupak, S.** 2005. Resistance to crack propagation of alloyed structural and cast steels, Mechanika 4(54): 12-17.
8. Standard Test Method for Plane-Strain Fracture Toughness of Metallic Materials. ASTM E 399-83. 30p.
9. **Leonavičius, M.K.; Petraitis, G.; Selivonec, J.** 2011. Resistance to cyclic loading. Vilnius: Technika. 184p. (in Lithuanian).
10. **Maruschak, P.; Bishchak, R.; Baran, D.; Poberezhny, L.** 2013. Failure analysis of continuous casting rolls material and physical simulation of thermal fatigue loading, Mechanika 19(4): 398-402. http://dx.doi.org/10.5755/j01.mech.19.4.5046.
11. **Šadreika, P.; Žiliukas, A.** 2014. Determination of mixed-mode fracture characteristics due dynamic opening and in-plane shear cases, Mechanika 20(2): 135-139. http://dx.doi.org/10.5755/j01.mech.20.2.6936.

M. Leonavičius, E. Stupak, G. Petraitis

SKIRTINGAI TERMIŠKAI APDOROTO PLIENO MECHANINĖS SAVYBĖS IR CIKLINIS IRIMAS

R e z i u m ė

Pateiktos skirtingai termiškai apdoroto vidutinio anglingumo mažai legiruoto plieno AISI 4130 statinės mechaninės, dinaminės ir atsparumo cikliniam apkrovimui savybės. Nežymus cheminės sudėties pokytis ir terminio apdorojimo procesas pakeičia kietumą, stiprumą, plastines savybes, smūginį tąsumą ir ciklinio irimo plyšėjimo slenkstį. Atlikta CT bandinių lūžių analizė SEM pagalba parodo ryšį tarp medžiagos struktūros ir ciklinio irimo proceso.

M. Leonavičius, E. Stupak, G. Petraitis

MECHANICAL PROPERTIES AND CYCLIC FRACTURE BEHAVIOR OF DIFFERENTLY HEAT-TREATED STEEL AISI 4130

S u m m a r y

Static mechanical, dynamic and resistance to cyclic loading properties obtained for differently heat-treated low carbon steel AISI 4130. Insignificant change of chemical content and heat-treatment change hardness, strength, ductility properties, impact resistance and threshold value of fatigue crack propagation. An analysis of CT specimens' fractured views performed using SEM shows relationship of material microstructure with cyclic fracture.

Keywords: steel, heat-treated, fatigue, fracture.

Received April 07, 2014
Accepted September 17, 2014